Numerical Simulation of Evaporating Capillary Jets

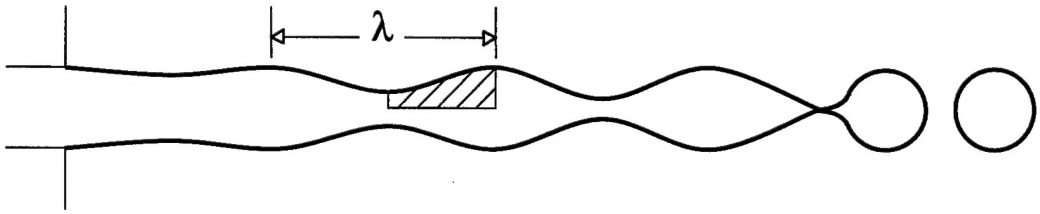

by

Jason D. Zeda

A major report submitted to the
Department of Mechanical Engineering
of the University Of Hawaii at Manoa
in partial fulfillment of the requirements for the degree of

Master of Science

August 1999

DISTRIBUTION STATEMENT A
Approved for Public Release
Distribution Unlimited

19990827 086

DTIC QUALITY INSPECTED 4

To my wife Sheila and daughter Chelsea

And especially my Lord and Savior Jesus Christ

ABSTRACT

Numerical Simulation of Evaporating Capillary Jets

Jason D. Zeda

Advisor: Dr. Farzad Mashayek

A detailed numerical study of evaporating capillary jets is presented. The analysis is performed through use of a Galerkin finite element method with penalty formulation for solving the equations of motion and a flux method for tracking the free surface.

A parametric study is performed to analyze the temporal instability of the evaporating jet. Through varying the evaporation rate, Reynolds number, disturbance wavenumber, initial disturbance amplitude, and density ratio the outcomes of jet breakup are investigated. Also, pressure distribution inside the jet and multiple satellite drop formations are analyzed. Results are compared to existing analytical conclusions made from linear stability analysis.

This study reveals that surface evaporation has a destabilizing effect for the low-speed jets, which are considered here. That is, evaporation flux is greater at the neck than the crest, which accelerates the wave growth. Satellite drops also reduce in size as evaporation rate is increased. This reduction is seen in both the radial direction due to vapor leaving the surface and along the axis of symmetry due to decreased breakup time.

Acknowledgements

I would like to reveal my sincere appreciation to my advisor Dr. Farzad Mashayek for his eagerness and dedication in supporting my one-year pursuit of a master's degree. Although this task was unusual and difficult, during the entire operation he implanted faith in me that it could be done.

Thanks also to Drs Choa and Teng for reviewing my major report and being members of my examination committee.

Without a doubt, I owe the United States Navy for allowing me the opportunity to relax my military obligations and to fulfill this lifelong goal. Of course, I have deep gratitude for their financing of this entire year of studies.

Most of all I am indebted to the Lord for his unending grace and mercies upon sinners like you and me. For we all fall short of the glory of God and need Jesus to intercede between us and the Father.

Table of Contents

Abstract	i
Acknowledgements	ii
Table of Contents	iii
List of Figures	iv
Nomenclature	v
1. Introduction	1
2. Formulation and Methodology	4
3. Effect of Evaporation on Jet Instability	11
3.1 Location of the breakup point	12
3.2 Growth rate of the disturbances	15
3.3 Breakup time and volume	20
3.4 Drop size at breakup	23
3.5 Evaporation Flux on the free surface	24
3.6 Pressure and velocity distributions	26
4. Conclusion	29
References	31

List of Figures

Figure #	Description	Page
1	Fluid subvolumes represented by their height and thickness	7
2	Time evolution of the instability: *Re*=200	12
3	Time evolution of the instability: *Re*=10	13
4	Motion of the minimum radius along the jet axis	14
5	Variation of the amplitude of the neck, swell, and their difference	16
6	Growth rate of disturbances	18
7	Breakup time of jet	21
8	Breakup volume of jet	22
9	Variation of drop size at breakup	23
10	Variation of the curvature of the jet	25
11	Pressure distribution and velocity vectors for a non-evaporating jet	27
12	Pressure distribution and velocity vectors for an evaporating jet	28
13	Formation of multiple satellite drops for a non-evaporating jet	29
14	Formation of multiple satellite drops for an evaporating jet	29

Nomenclature

C_p	specific heat
h	height function
$\mathbf{I}$	identity matrix
k	wavenumber
K	jet curvature
l	length
L_v	latent heat of vaporization
$\dot{m}$	evaporation flux
$\mathbf{n}$	outward unit normal
N	shape factor
p	pressure
Pr	Prandtl number
$\dot{Q}$	evaporation rate/length
r	radial coordinate
R	instantaneous radius
Re	Reynolds number
s	density ratio
t	time
T	temperature
$\mathbf{T}$	Newtonian stress tensor
u	jet axial velocity
U	free stream velocity
v	radial velocity
$\mathbf{v}$	velocity vector
V	volume
$\mathbf{w}$	velocity vector
We	Weber number
z	axial coordinate
Z	Ohnesorge number
β	dimensionless evap. rate
Γ	surface area of element
δ	change in
ε	disturbance amplitude
η	surface wave height
κ	thermal conductivity
λ	wavelength
ν	kinematic viscosity
ρ	density
σ	surface tension coefficient
τ	stress tensor
ω	growth rate
Ω	volume of element

Subscripts

b	boiling
c	curvature
e	element
g	gas
i,j	node number
l	liquid
n	neck
s	swell, surface
z	derivative
0	initial value

1. Introduction

The instability of liquid jets has been a classical fluid mechanics problem for more than a century. Early investigations focused primarily on understanding the mechanisms of jet breakup while recent jet instability studies have concentrated on more accurate predictions of growth rate, drop size after breakup, and effects due to variations in initial disturbance amplitude, disturbance type, and fluid properties. Despite extensive previous studies cited in the literature and briefly reviewed below, it has been only recently that the dynamics of a jet undergoing surface evaporation has been investigated by Lian and Reitz (1993) using a linear stability analysis. While this study reveals several new and interesting phenomena, it is, understandably, unable to predict accurate results near the breakup point due to the assumption of infinitesimal perturbation of the liquid jet.

The objective of the present work is to relax some of the assumptions adopted by Lian and Reitz (1993) and to provide a more versatile computational analysis of evaporating jets by implementing a Galerkin finite element method in conjunction with a height flux method (HFM) for interface tracking, which was developed by Mashayek and Ashgriz (1993). The dimensionless continuity and momentum equations are solved on a moving mesh consisting of four-node quadrilateral elements. Considering an axisymmetric incompressible Newtonian liquid jet of infinite length initially subjected to a periodic surface disturbance a parametric study is performed to show how evaporation affects capillary jet instability while varying liquid Reynolds number (Re), disturbance wavenumber (k), disturbance amplitude (ε_o), evaporation rate (β), and density ratio (s). Similar to Lian and Reitz we focus on the temporal evolution of the jet thus only one wavelength is examined at a time - in practice, we solve for only one half of this wavelength due to the symmetry of the jet. Also similar to Lian and Reitz (1993), the surface

evaporation of the perturbed jet is approximated by that of a spherical drop with the identical curvature as the local surface curvature of the jet. In this manner, there is no need to solve for the gas phase.

The observation that a liquid jet issuing from a nozzle will eventually breakup into small drops when subjected to even minute disturbances led Rayleigh (1879) to provide the first analytical description for the temporal instability of an inviscid, incompressible jet using a normal mode analysis. He showed that an axisymmetric harmonic disturbance of the form:

$$\eta = \varepsilon_o \exp(\omega t - ikz), \tag{1}$$

would grow in time according to:

$$\omega = \left[\frac{I_1(k)}{I_o(k)} \left(1 - k^2\right) k \right]^{1/2}, \tag{2}$$

where ω is the growth rate, t is the time, and I_o and I_1 are the modified Bessel functions of the first kind. In (1) and (2), length and time variables have been non-dimensionalized by r_o and r_o/v_e, where v_e is the capillary-wave velocity $(\sigma/\rho r_o)^{1/2}$. Here, r_o is the undisturbed radius of the jet, σ is the liquid surface tension coefficient, and ρ is the density of the liquid. This result predicts that disturbances grow in time for $k<1$ and oscillate for $k>1$, and the maximum growth rate occurs at $k=0.697$. In other words, if the wavelength ($\lambda=2\pi r_o/k$) of an axisymmetrical disturbance is greater than the cylinder circumference the jet will be unstable and if the disturbance wavelength is less than the cylinder circumference the jet will be stable.

For over a century since Rayleigh noticed that surface tension had to work against inertia in causing instability researches have continued to extend his work in both theoretical and experimental realms. For example, viscous effects have been considered by Weber (1931), who analyzed the motion of thin sections of fluids, and Chandrasekhar (1961), whose book focused

solely on the subject of instability using the Navier-Stokes equation to examine it. To test the results of linear theory quantitative experiments were performed by such researchers as Goedde and Yuen (1970). The experiments clearly identified that drop size varied at breakup leading to the conclusion that nonlinear behavior became dominant during instability. Yuen (1968) was the first to extend Rayleigh's linear analysis by considering a third-order perturbation expansion, which would give some explanation of the production of satellite drops between the larger main drops. Further experimental investigation of both satellite and main drops have been done by Vasallo and Ashgriz (1991) and Kowalewski (1996), which looked at the production of multiple satellites and the description of the jet surface near breakup, respectively.

Due to recent development of computational facilities and numerical techniques flow simulations have become common place. Inviscid flow was studied by Mansour and Lundgren (1990) and Stokes flow has been considered by Stone and Leal (1989). These two simplifying factors breakdown close to breakup because both viscous and inertial effects become important. In this case the full Navier-Stokes equation has to be considered in the fluid domain. A finite difference one-dimensional model was considered by Eggers and Dupont (1994) to simulate drop formation. The most extensive study of jet breakup using the Navier-Stokes equation was performed by Ashgriz and Mashayek (1995) using a Galerkin finite element method. For a review of the computational methods used for free surface flows see Tsai and Yue (1996). Further reviews of the problem of jet instability are given by Bogy (1979) and more recently by Eggers (1997).

Unfortunately, little mention is made about evaporating jets when studying the problem as a whole. This is primarily due to the complexity of determining an evaporation equation for

an irregular shaped surface. Hopefully future experimentation will be performed to verify the spherical model used herein.

2. Formulation and Methodology

Consider a viscous liquid circular jet injected with velocity U into an inviscid gas at temperature T_∞, in zero gravity. Since we are dealing with interactions of the gas with only one jet, it can be assumed that the total heat capacity of the gas is much larger than that of the liquid and T_∞, far from the surface of the jet, is constant. The implementation of an evaporation model, described below, eliminates the need for the solution of the energy equation; thus the governing equations include only mass and momentum conservations. Assuming both the liquid and the gas are incompressible with constant properties, these equations are described as:

$$\nabla \cdot \mathbf{w}_i = 0, \tag{3}$$

$$\frac{\partial \mathbf{w}_i}{\partial t} + \mathbf{w}_i \cdot \nabla \mathbf{w}_i = -\frac{1}{\rho_i} \nabla p_i + \nu_i \nabla^2 \mathbf{w}_i, \quad i = l, g \tag{4}$$

where l and g stand for liquid and gas, respectively. In (3) and (4), $\mathbf{w}$, p, ρ, and ν denote the velocity, pressure, density, and kinematic viscosity, respectively. For a liquid jet evaporating with a flux $\dot{m}$, the jump condition and the normal stress balance on the interface are given by (Lian and Reitz, 1993):

$$\dot{m} = \rho_l (\mathbf{w}_l - \mathbf{w}_s) \cdot \mathbf{n} = \rho_g (\mathbf{w}_g - \mathbf{w}_s) \cdot \mathbf{n}, \tag{5}$$

$$\dot{m}(\mathbf{w}_g - \mathbf{w}_l) \cdot \mathbf{n} + [\mathbf{n} \cdot (\tau_g - \tau_l)] \cdot \mathbf{n} + \sigma \nabla \cdot \mathbf{n} = 0, \tag{6}$$

where σ, τ, $\mathbf{w}_s$, and $\mathbf{n}$ denote the surface tension coefficient, the stress tensor including the pressure component, the interface velocity, and the outward unit normal, respectively. The first

term on the left-hand side of (6) is the recoil force on the jet due to surface evaporation. This force stems from a net momentum that is impacting the surface. Eliminating $\mathbf{w}_s$ in (5) yields:

$$\left(\mathbf{w}_g - \mathbf{w}_l\right)\cdot\mathbf{n} = \frac{\dot{m}}{\rho_g}\left(1 - \frac{\rho_g}{\rho_l}\right). \tag{7}$$

In this study we consider $\rho_g << \rho_l$, therefore the effects of the fluctuations in the ambient gas pressure may be neglected in comparison to the effects of the pressure fluctuations in the liquid. Further, the mean pressure of the gas affects only the mean pressure of the jet and, for incompressible liquid, does not influence the instability of the jet. As a result, we can neglect the ambient gas pressure and, for inviscid gas, eliminate τ_g from (6). Then, by implementing (7), (6) yields:

$$\mathbf{n}\cdot\tau_l\cdot\mathbf{n} = \sigma\nabla\cdot\mathbf{n} + \frac{\dot{m}}{\rho_g}. \tag{8}$$

This simplifies the problem significantly, as there will be no need to solve for the gas phase. It must be noted that, in this manner the mean pressure of the jet is calculated relative to the mean pressure of the ambient gas.

There is no analytical solution for evaporation of a jet with a perturbed surface. However, following Lian and Reitz (1993) one may approximate the unit area evaporation rate of a wavy curved surface of local radius of curvature R_c with that of a sphere of the same radius. In this study, assuming that the surface temperature of the jet is always at the boiling temperature T_b, the flux of evaporation is modeled as:

$$\dot{m} = \frac{\dot{Q}}{R_c} \quad for\ R_c > 0, \tag{9}$$

where,

$$\dot{Q} = \frac{1}{2}\left(\frac{\kappa_g}{C_{pg}}\right)\ln\left[1+\frac{C_{pg}\left(T_\infty - T_b\right)}{L_v}\right]\left(1+0.276\,Re_g^{\,1/2}Pr_g^{\,1/3}\right), \tag{10}$$

where κ, C_p, and L_v denote the thermal conductivity, the specific heat, and the latent heat of evaporation, respectively. The Reynolds number, Re, and the Prandtl number, Pr, are defined as $Re_g=2Ur_o/\nu_g$ and $Pr_g=\rho_g\nu_gC_{pg}/\kappa_g$. Equations (9) and (10) are a modified form of the d^2-law for evaporation of a single drop in zero gravity (Williams 1985 and Turns 1996). The modification, here, is by substituting the local radius of curvature of the perturbed jet for the radius of the spherical drop. This modification was first introduced by Lian and Reitz (1993). The physical reasoning is that the surface of the deformed jet may be "locally" considered as the surface of a spherical drop having the same radius of curvature. It is noted that the utilization of (9) is limited to surface deformations such that $R_c > 0$.

In the remaining equations (for the liquid phase) an axisymmetric incompressible Newtonian liquid jet in zero gravity is considered. The variables are non-dimensionalized by the undisturbed jet radius r_o, and the characteristic time $(\rho r_o^3/\sigma)^{1/2}$. The dimensionless continuity and momentum equations are:

$$\nabla\cdot\mathbf{v} = 0, \tag{11}$$

$$Re\left(\frac{\partial\mathbf{v}}{\partial t} + \mathbf{v}\cdot\nabla\mathbf{v}\right) = \nabla\cdot\mathbf{T}, \tag{12}$$

where $\mathbf{v}\equiv\mathbf{w}_l=(u,v)$ is the velocity vector and $\mathbf{T}\equiv\tau_l=-p\mathbf{I}+[\nabla\mathbf{v}+(\nabla\mathbf{v})^T]$ is the stress tensor for a Newtonian fluid with p now denoting the normalized liquid pressure. The Reynolds number in (12) is defined as $Re=(1/\nu_l)(\sigma r_o/\rho_l)^{1/2}$. Non-dimensionalizing (8) the stress balance on the interface yields:

$$\mathbf{T}\cdot\mathbf{n} = Re\left(K+\alpha K^2\right)\mathbf{n}, \tag{13}$$

where K is the curvature of the surface and

$$\alpha = \frac{\beta}{s}, \quad \beta = \frac{\dot{Q}}{(\rho_l r_o \sigma)^{\frac{1}{2}}}, \quad s = \frac{\rho_g}{\rho_l}. \tag{14}$$

As a result of the non-dimesionalization, the parameters affecting the instability of an evaporating jet reduce to Reynolds number Re, the dimensionless evaporation rate β, and the density ratio s. In the next section we investigate the effects of these parameters as well as the effects of initial disturbance amplitude ε_o and wavenumber k via numerical simulation.

In this investigation it is assumed that the free surface can be represented by a height function $h(z,t)$, as shown in Fig. 1, thus the curvature K is calculated using:

$$K = \frac{h_{zz}}{\left(1+h_z^2\right)^{3/2}} - \frac{1}{h\left(1+h_z^2\right)^{1/2}}. \tag{15}$$

Since a temporal analysis is considered symmetry boundary conditions can be applied on the axis and planes of symmetry:

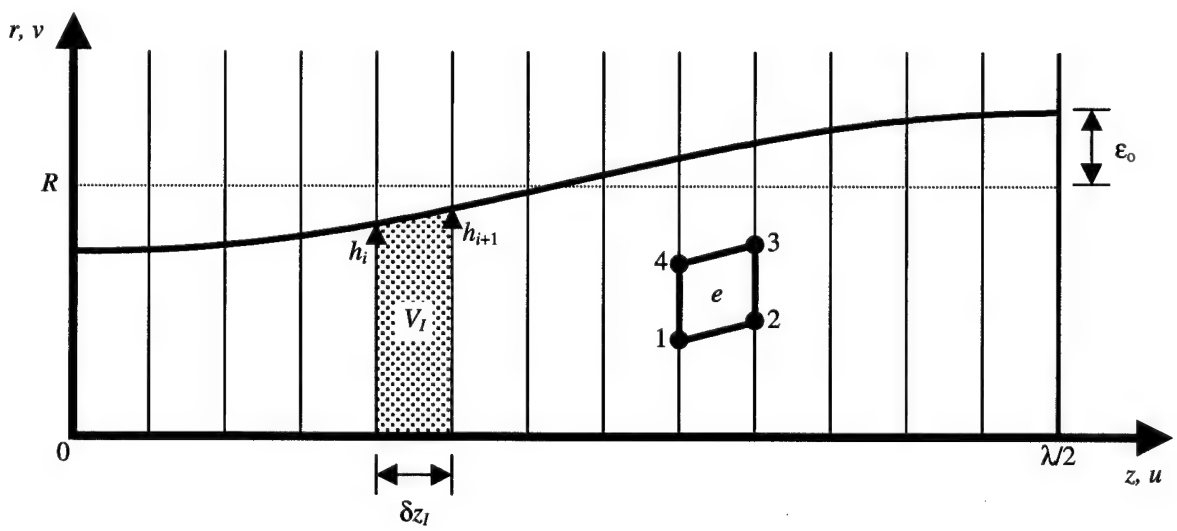

Figure 1: Fluid subvolumes represented by their height and thickness.

$$\frac{\partial u}{\partial r} = 0 \text{ and } v = 0, \text{ at } r = 0 \tag{16}$$

$$u = 0 \text{ and } \frac{\partial v}{\partial z} = 0, \text{ at } z = 0, \frac{\lambda}{2}. \tag{17}$$

A Galerkin finite element method is used to solve (11) and (12). Using a penalty function formulation (Hughes, Liu and Brooks 1979), the pressure term is eliminated from the set of unknown variables by absorbing the continuity equation into the momentum equation. In this formulation the pressure is defined as:

$$p = -\mathrm{Y}\nabla \cdot \mathbf{v}, \tag{18}$$

where Y is a large number of order (10^9) depending on viscosity and Reynolds number. Four-node bilinear isoparametric elements are used to approximate the velocity distribution over each element:

$$\mathbf{v}(r,z,t) = \sum_{i=1}^{4} \mathbf{v}_i(t) N_i(r,z,t). \tag{19}$$

A moving mesh is considered to discretize the computational domain making the shape functions, N_i, time dependent. In order to obtain the finite element formulation, (12) is multiplied by the shape function N_j and integration is carried over the element volume. After the divergence theorem is invoked the resulting equation is:

$$\int_{\Omega(t)} \left(N_j Re \left(\frac{\partial \mathbf{v}}{\partial t} + \mathbf{v} \cdot \nabla \mathbf{v} \right) + \nabla N_j^T \cdot \left[-p\mathbf{I} + \left[\nabla \mathbf{v} + (\nabla \mathbf{v})^T \right] \right] \right) d\Omega = \int_{\Gamma(t)} N_j \mathbf{T} \cdot \mathbf{n} \, d\Gamma, \tag{20}$$

where Ω is the volume and Γ is the surface area of the element. Through substitution of (13) and (18) into (20) we obtain the following closed form finite element formulation:

$$\int_{\Omega(t)} \left(N_j Re \left(\frac{\partial \mathbf{v}}{\partial t} + \mathbf{v} \cdot \nabla \mathbf{v} \right) + \nabla N_j^T \cdot \left[\mathrm{Y}(\nabla \cdot \mathbf{v})\mathbf{I} + \left[\nabla \mathbf{v} + (\nabla \mathbf{v})^T \right] \right] \right) d\Omega = \int_{\Gamma(t)} N_j Re\left(K + \alpha K^2\right) \mathbf{n} \, d\Gamma. \tag{21}$$

The above formulation is based on a fixed mesh. In the present problem the mesh is moving, therefore special treatment of the time derivatives is required. Since the shape function is time dependent, the time derivative of velocity in discretized form becomes:

$$\left(\frac{\partial \mathbf{v}}{\partial t}\right)_{r,z} = \sum_{i=1}^{4} \frac{d\mathbf{v}_i}{dt} N_i + \sum_{i=1}^{4} \mathbf{v}_i \left(\frac{\partial N_i}{\partial t}\right)_{r,z}. \tag{22}$$

The last term of (22) introduces a new convective term in (21). Here, we allow the motion of the nodes in the r-direction only, according to the following simple rule:

$$z_i(t+\delta t)=z_i(t)=\text{constant}, \quad r_i(t+\delta t)=cr_i(t), \tag{23}$$

where the subscript i refers to the node number, and $c=c(z,t)$ is a constant for each column of nodes in the radial direction defined as:

$$c = h(z,t+\delta t)/h(z,t). \tag{24}$$

In this case, Mashayek and Ashgriz (1993) have shown that the total derivative of velocity becomes:

$$\frac{D\mathbf{v}}{Dt} = \frac{\partial \mathbf{v}}{\partial t} + \left(v - \frac{c-1}{\delta t} r\right)\frac{\partial \mathbf{v}}{\partial r} + u\frac{\partial \mathbf{v}}{\partial z}. \tag{25}$$

Substitution of (25) into (21) completes the finite-element formulation for the present problem.

The free surface of the jet is determined using the Height Flux Method (HFM) developed by Mashayek and Ashgriz (1993). As shown in Fig. 1 the domain is divided into several vertical subvolumes of width δz_I and volume V_I. The location of the free surface on the left and right hand sides of a subvolume is given by h_i and h_{i+1} at time t, respectively. At the end of each time step fluxes of the fluid from each subvolume to its neighboring subvolumes are calculated using the velocity field determined by the finite element solution of the governing equations. Next, with the knowledge of the evaporation rate, the volume change δV_e of each subvolume due to evaporation at the interface is calculated using:

$$\delta V_e = 2\pi\left(\frac{h_{i+1}+h_i}{2}\right)K\,\beta\,\delta l\,\delta t\,, \tag{26}$$

where δl indicates the length of the interface confined within the subvolume. The volume of fluid within each subvolume is further modified by calculating the flow through the side planes. Then, it is assumed that the part of the interface located between any neighboring pair of subvolumes can be approximated by a line segment described as $h=az+b$, where a and b are constants which can be determined by the known volumes. More details and the accuracy of this method are discussed by Mashayek and Ashgriz (1993).

Mesh Size	4 x 30	4 x 40	4 x 50	4 x 60
Growth Rate	0.712	0.712	0.712	0.712

Table 1: Typical convergence test for growth rate: Re=200, ε_o=0.05, k=0.7, β=3x10^{-2}, and s=10^{-3}.

Before numerical results were compiled a convergence study was performed to determine the effect of mesh size on growth rate. The results are shown in table 1. From this we conclude that grid size does not affect growth rate since only the height of the free surface at the neck and swell where of importance for calculating this value. To save computational time the majority of cases were ran with a minimal number of elements. The mesh size for the determination of growth rate was limited to four elements in the radial direction and the axial elements were changed based on the wavenumber as given in table 2. For the cases where pressure distribution and velocity vectors were plotted the grid was refined in order to obtain better print quality and color dispersion.

Wavenumber	0.3	0.4	0.5	0.6	0.7	0.8	0.9
Number of elements	50	40	40	30	30	20	20

Table 2: Number of axial elements used in simulations for determination of growth rate.

3. Effect of Evaporation on Jet Instability

We consider the temporal evolution of a liquid jet, initially at rest with a spatially harmonic surface described as:

$$r=R-\varepsilon_o\cos(kz), \tag{27}$$

where R is determined such that the volume of the jet is kept constant when the initial amplitude is changed:

$$R=\left(1-\tfrac{1}{2}\varepsilon_o^2\right)^{1/2}. \tag{28}$$

Due to symmetry, only half a wavelength is considered. The trough (neck) of the initial surface is set at z=0 and the crest (swell) at $z=\lambda/2$. The dynamics of this jet due to capillary and recoil forces are investigated for various values of dimensionless evaporation rate, density ratio, Reynolds number, disturbance wavenumber, and initial disturbance amplitude.

Detailed description of the shape evolution of liquid jets with Re=200 and 10 is presented in Figs. 2 and 3 for k=0.7,0.4 and β=0, 10^{-2}, and 3×10^{-2}. The following characteristics for the breakup of an evaporating capillary jet can be observed from Figs. 2 and 3: (i) As evaporation rate increases the breakup time decreases; (ii) As Reynolds number decreases the breakup time increases; (iii) The length and diameter of the liquid ligament decreases with increasing evaporation rate and decreasing Reynolds number; (iv) The breakup point is closer to the initial trough as evaporation rate increases, due to the decrease in time that nonlinear effects can influence jet breakup. A more detailed description of these characteristics is given in the following sections.

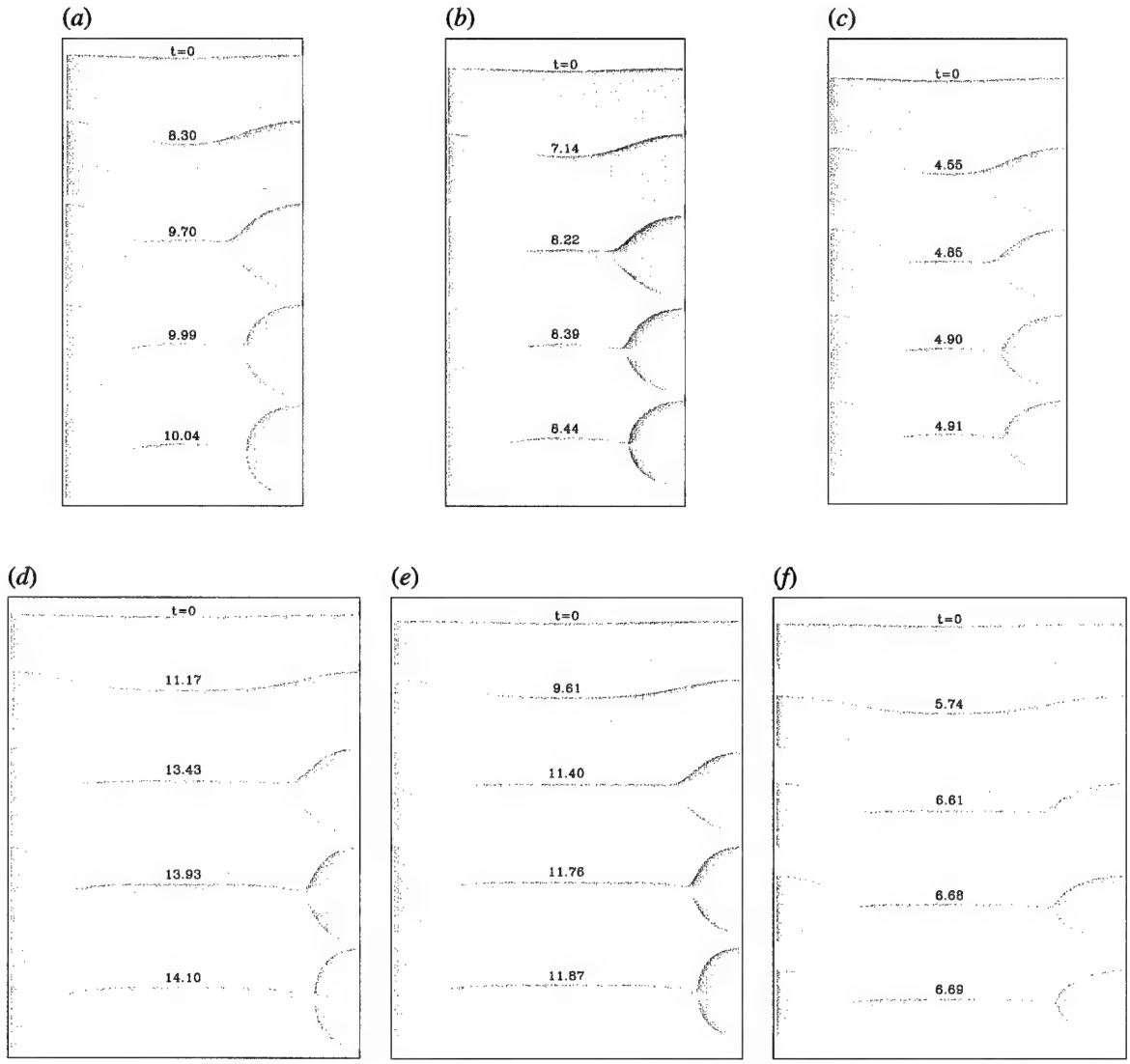

Figure 2: Time evolution of the instability, Re=200, ε_o=0.5, s=10^{-3}: (*a*) k=0.7, β=0; (*b*) k=0.7, β=10^{-2}; (*c*) k=0.7, β=3x10^{-2}; (*d*) k=0.4, β=0; (*e*) k=0.4, β=10^{-2}; (*f*) k=0.4, β=3x10^{-2}.

3.1 Location of the breakup point

Linear theory predicts that the breakup point is always at the trough of the initial disturbance where the initial jet radius is minimum. However, Figs. 2 and 3 clearly show that the

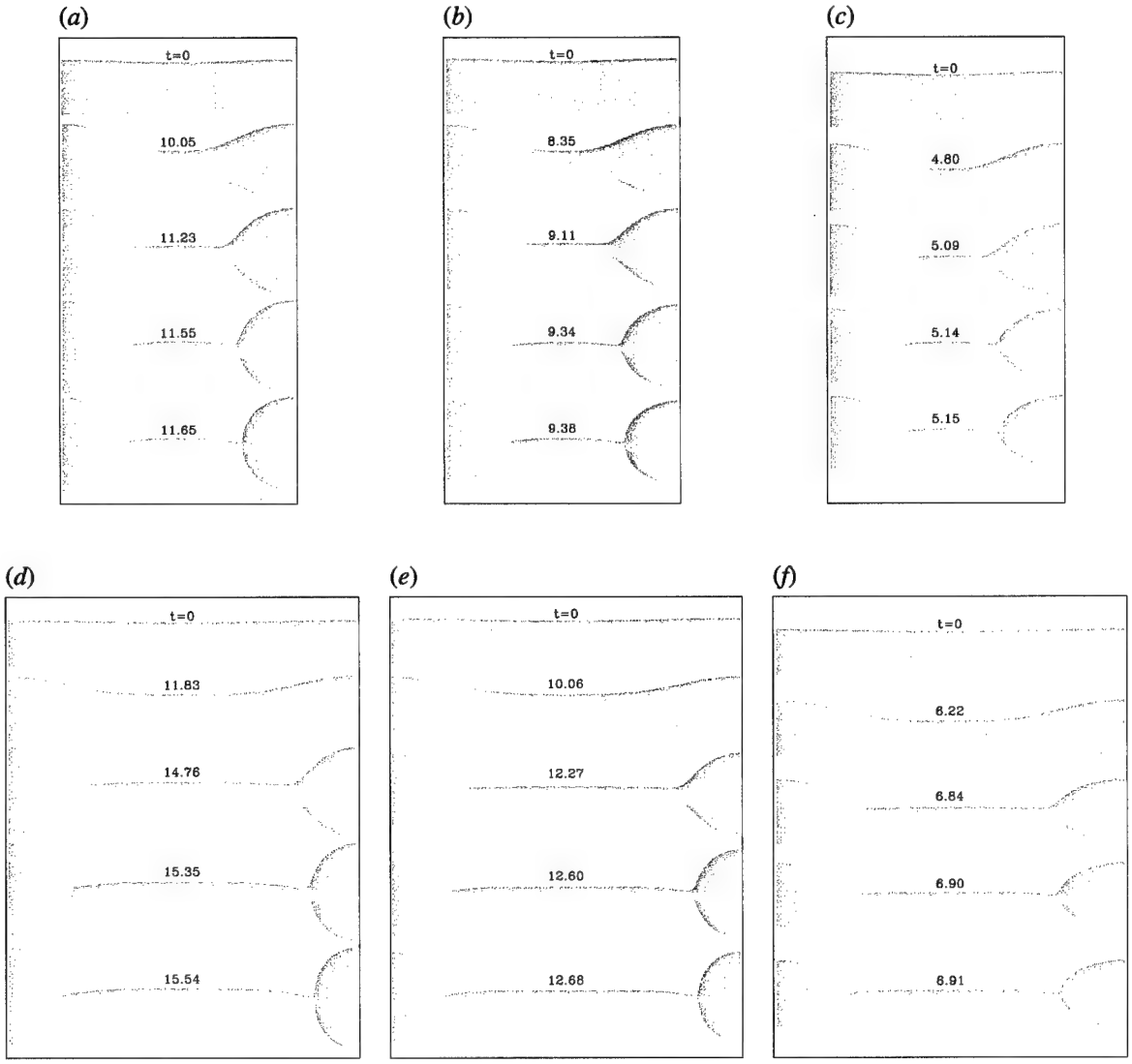

Figure 3: Time evolution of the instability, Re=10, ε_o=0.5, s=10^{-3}: (*a*) k=0.7, β=0; (*b*) k=0.7, β=10^{-2}; (*c*) k=0.7, β=3x10^{-2}; (*d*) k=0.4, β=0; (*e*) k=0.4, β=10^{-2}; (*f*) k=0.4, β=3x10^{-2}.

breakup point moves in the direction of the swell towards the end of the simulation. The capillary forces on the jet tend to "squeeze" the liquid in the neck region into the swell. This results in the formation of two distinct regions in the jet. The middle region where the curvature in the r-z plane is very small, resembling a liquid ligament, and the swell region where the curvature in the r-z plane is large. Note from Figs. 2 and 3 that the disturbances stay sinusoidal

for a very long time (relative to the breakup time) and agree with linear theory until non-linear effects begin to move the location of the minimum radius.

In order to gain a better understanding of the development of the breakup point of the jet, we have plotted the motion of the minimum radius along the jet from time t=0 to the breakup time. This plot is shown in Fig. 4 for a jet with Re=200, ε_o=0.05, s=10^{-3}, and for three different evaporation rates. Two distinct time periods can be identified for each of the curves in these

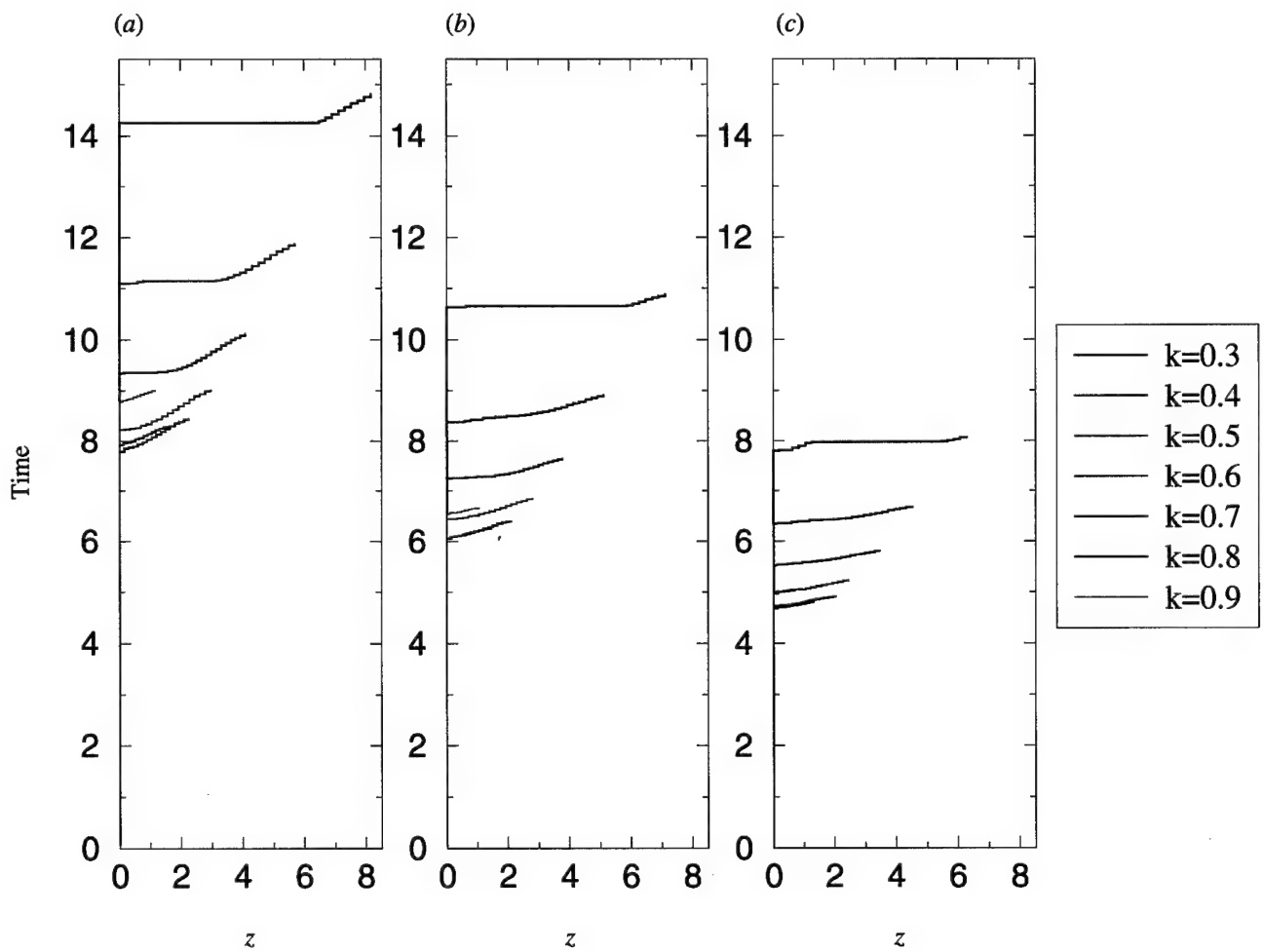

Figure 4: Motion of the minimum radius along the jet axis: (*a*) $\beta=10^{-2}$; (*b*) $\beta=2\text{x}10^{-2}$; (*c*) $\beta=3\text{x}10^{-2}$.

figures. The most important being the time that the minimum point stays at z=0. This time represents over 90% of the total breakup time in all cases and it first reduces and then increases with an increase in the wavenumber. The case with the maximum disturbance growth rate is the first to begin movement away from z=0. The second distinct time period represents the rapid movement of the minimum jet radius from the neck towards the swell region. This sudden relocation of minimum point in the axial direction is larger for smaller wavenumbers. The end points on all the curves in Fig. 4 represent the breakup times. There are two interesting features to note from Fig. 4. The first is that as evaporation rate increases the location of the minimum point is closer to the neck for each wavenumber. This represents the production of a smaller middle ligament or satellite drop. The second feature reveals that as evaporation rate increases the range of time that each wavenumber breaks away from z=0 reduces.

3.2 Growth rate of the disturbances

Linear theory not only defines the region of unstable disturbance wavenumbers but also provides their growth rates. These growth rates are useful in estimating the breakup time and length. According to linear theory the variation of the logarithmic value of the amplitude of the surface disturbances with time is linear. However, for an actual liquid jet this amplitude variation is nonlinear at the beginning of the simulation due to the fact that radial velocity of the jet starts from zero. The amplitude variation is nonlinear also near the breakup point due to the movement of the minimum radius. For a selected few of our simulations we have plotted the logarithmic values of the normalized amplitudes of the neck ($(R_e-r_n)/\varepsilon_o$), swell ($(r_s-R_e)/\varepsilon_o$), and their difference ($(r_s-r_n)/\varepsilon_o$) in Fig. 5. Here, r_n and r_s are the radii of the neck and swell,

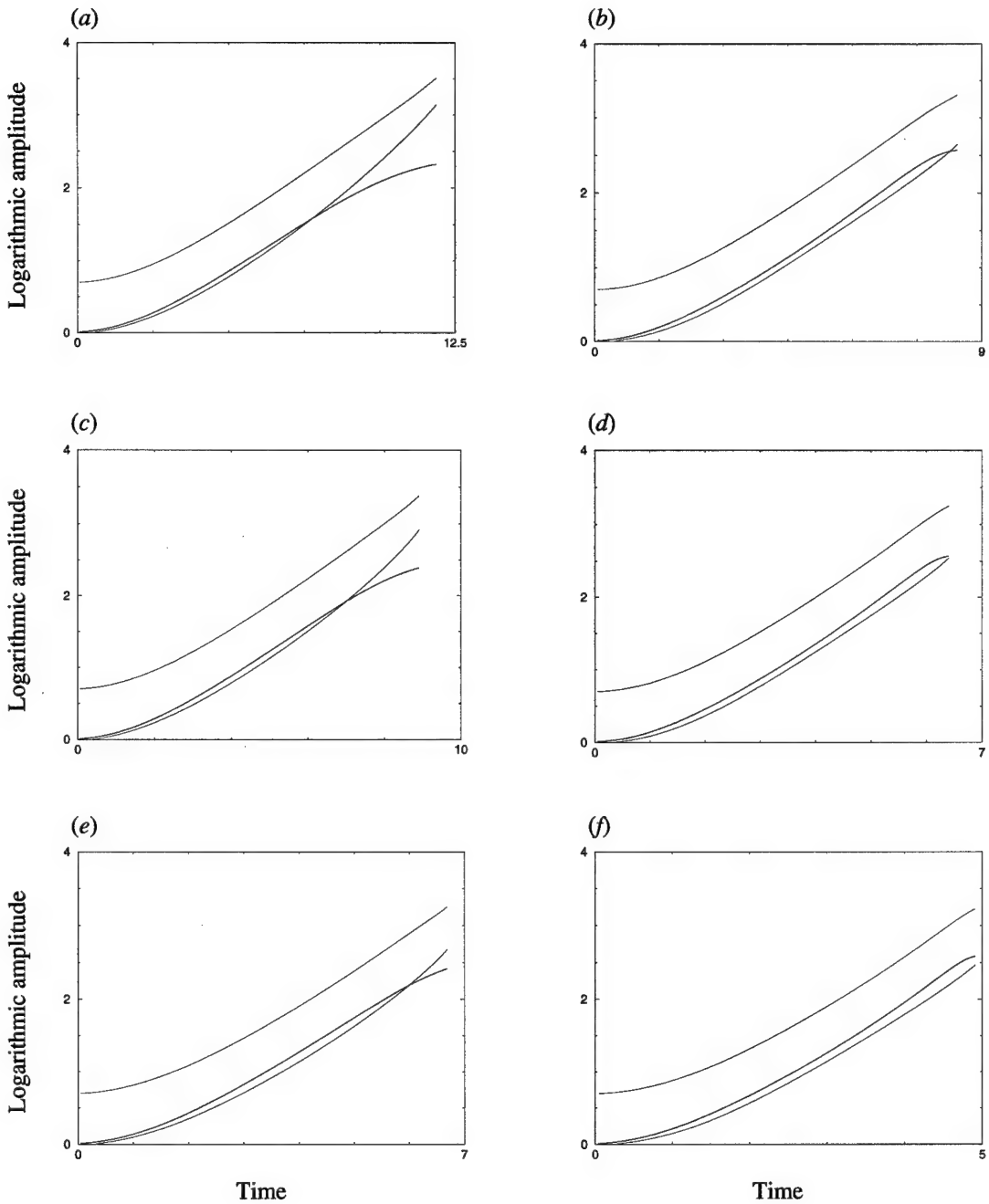

Figure 5: Variation of the amplitude of the neck (black), swell (red), and their logarithmic difference (green), Re=200, ε_o=0.5, s=10^{-3}: (*a*) k=0.4, β=10^{-2}; (*b*) k=0.7, β=10^{-2}; (*c*) k=0.4, β=2x10^{-2}; (*d*) k=0.7, β=2x10^{-2}; (*e*) k=0.4, β=3x10^{-2}; (*f*) k=0.7, β=3x10^{-2}.

respectively, and R_e is the instantaneous radius of the equivalent cylindrical jet, which changes during the simulation due to evaporation. Notice in Fig. 5 that the logarithmic variation of

amplitude of the neck or swell is not perfectly linear. Figure 5 reveals interesting features for the temporal evolution of amplitudes of the neck and the swell with respect to each other. Initially the growth rate of the neck point is larger than the growth rate of the swell point, since a radial displacement in the neck region corresponds to a smaller radial displacement in the swell region for the same volume displacement. Due to the formation of a liquid ligament, i.e. minimum radius point moving away from the neck, the growth rate of the amplitude of the neck decreases eventually dropping below that of the swell for the longer wavelengths. This is clearly shown in Fig. 5a,c,e, which also indicates that as we increase the evaporation rate the time after the cross point is reduced. This represents the formation of a smaller liquid ligament, which can be seen in Figs. 2 and 3. Figure 5b,d,f is representative of smaller disturbance wavelengths. Due to the reduced time of breakup non-linear effects are only visible in the last instances of instability. Comparing Fig. 5a,c,e with 5b,d,f we see that the shape of the difference curve varies only in slope when a change in wavenumber is made.

Similar to previous research in this area we use the linear region of the difference curve to provide values that can represent the growth rate for each wavenumber. Therefore, a line is fit to the difference between the amplitudes of the neck and swell and its slope is measured. The line is fit only to the middle region of each curve and the end portions are ignored. The dispersion curves are obtained using the calculated values of the growth rate for different wavenumbers and for various values of β, Re, ε_o, and s. The data are plotted in Fig. 6. As mentioned earlier Fig. 6a shows quantitatively that as we increase the evaporation rate the growth rate increases therefore reducing the time it takes for the jet to breakup into droplets. All curves in Fig. 6a give the maximum growth rate at k=0.7, similar to linear theory. Figure 6b presents the effects of Reynolds number on growth rate of disturbances. Here we can clearly

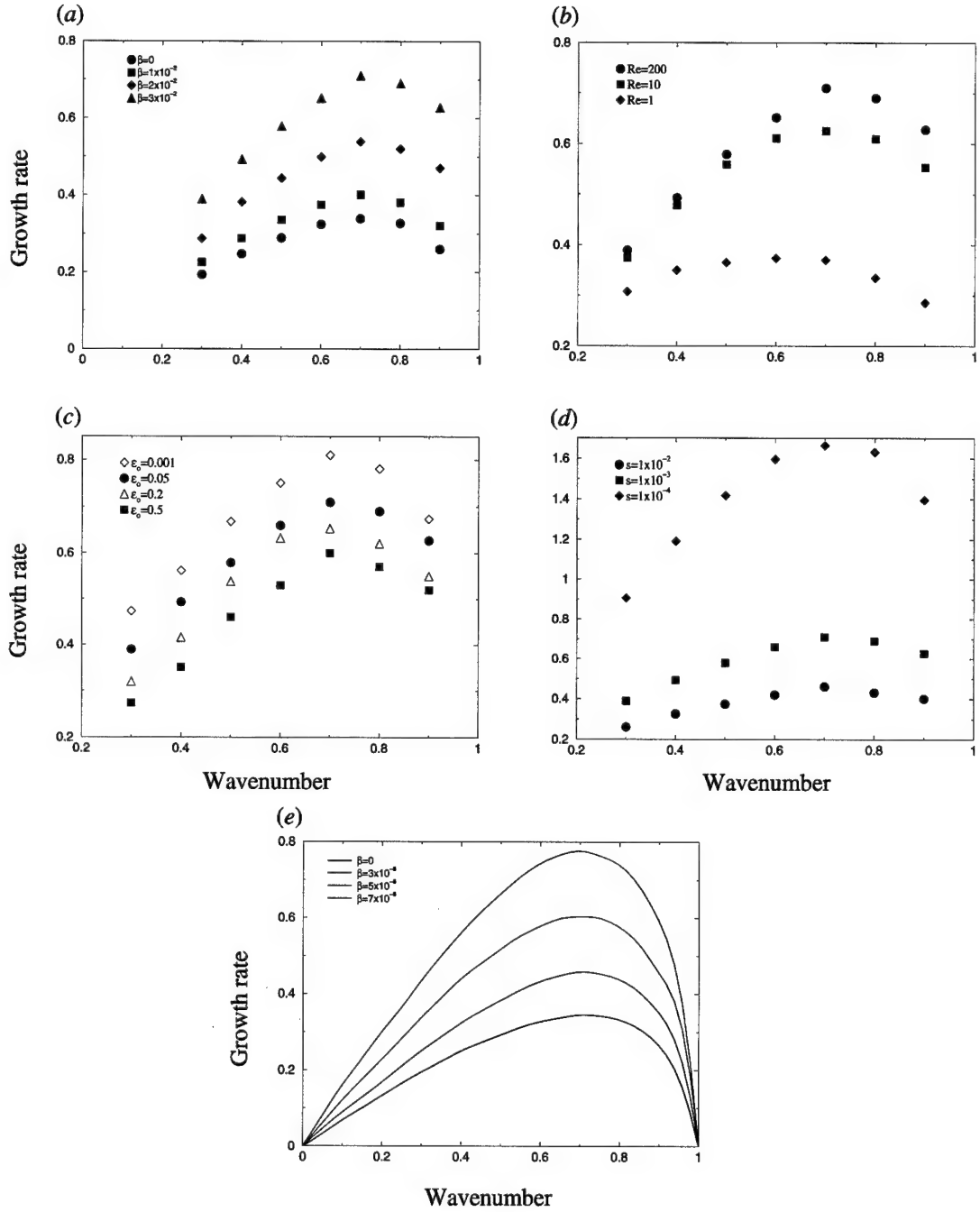

Figure 6: Growth rate of disturbances: (*a*) Re=200,ε_o=0.05,s=10^{-3}; (*b*) ε_o=0.05,β=3x10^{-2},s=10^{-3}; (*c*) Re=200,β=3x10^{-2},s=10^{-3}; (*d*) Re=200,ε_o=0.05,β=3x10^{-2}; (*e*) Lian & Reitz (1993).

identify for evaporating jets that as we decrease the Reynolds number the growth rate of disturbances decreases due to the more viscous nature of the jet not allowing the fluid to be

displaced as easily. Also from this graph we see a movement of the maximum growth to a lower wavenumber for the case of highly viscous fluids. Figure 6c demonstrates the effects of initial disturbance amplitude on growth rates. As mentioned earlier, linear theory assumes infinitesimal initial disturbance amplitude. Therefore, for large initial disturbance amplitudes the theoretical solutions result in large errors. We see from Fig. 6c that as we increase this value growth rate decreases at each wavenumber. However, this does not mean that the jet will take longer to breakup for large initial disturbance amplitudes. This figure only gives meaning to the rate and not the overall distance that the radius has to decrease in order to pinch off the jet. Figure 6d provides insight into the effect of the density ratio on growth rate. Here we clearly see that as we increase the density of the gas or decrease the density of the liquid (i.e. larger s) the growth rate of the evaporating jet decreases. This can be explained through the reduction of the recoil force, where the net momentum imparted on the surface is diminished by increasing s (see (13)).

Figure 6e shows the results from Lian and Reitz's (1993) linear stability analysis for an evaporating viscous jet with s=0.25x10^{-8}, We$_g$=10^{-4}, and Z=10^{-4}, where We$_g$ represents the Weber number and Z represents the Ohnesorge number. Since we do not solve for the gas phase we must convert their formulation to agree with our input parameters. For the case shown in Fig. 6e this would result in a Re=20,000 due mainly to their very small value for density ratio (e.g. s for air and water would be approximately 1.2x10^{-3}). Using this Reynolds number and similar values of s and β we attempted to correlate a direct comparison but was unable to reproduce their results. The calculated growth rates in our simulations were very similar to cases with no evaporation. Only when we increased β to around 5x10^{-5} did we obtain growth rates larger than that of non-evaporating cases. Although we could not reproduce the exact results from the analytical study, even using the same parameters, we both conclude the same general trends for

growth rate. As evaporation rate increases growth rate increases for every wavenumber. One possible reason for the discrepancies between our results and theirs is the linear theory's assumption of infinitesimal disturbance amplitude. For non-evaporating jets the growth rate does not vary up to an initial disturbance amplitude of approximately 0.05. However, Fig. 6c clearly shows that the growth rate varies in this region for evaporating jets. From this one may question the validity of the normal mode method for evaporating jets. Another possible reason for the differences can be tracked to their initial conditions where at t=0 the free surface is moving but there is no internal flow field. We could not produce such initial condition in our numerical simulations.

3.3 Breakup time and volume

Linear theory predicts that the minimum breakup time occurs at k=0.697, which corresponds to the wavenumber with the maximum growth rate. However, this is only true for $\varepsilon_o \rightarrow 0$, otherwise the minimum breakup time occurs at higher values of k as explained by Chaudhary and Redekopp (1980). In the simulations presented in Fig. 7a,b,c,d the initial disturbance amplitude equals 0.05 therefore most of our curves give a minimum breakup time for k=0.8. From Fig. 7a we can quantitatively deduce that as we increase the evaporation rate we decrease the breakup time, which has been demonstrated by other graphs presented earlier. This is due to the fact that the addition of recoil force has a destabilizing effect for low speed jets, which we are considering in this study. Also evaporation decreases the mean radius of our jet with time. Figure 7b clearly shows that as we decrease the Reynolds number breakup time increases, which is due to the additional viscous damping. This result is also in agreement with

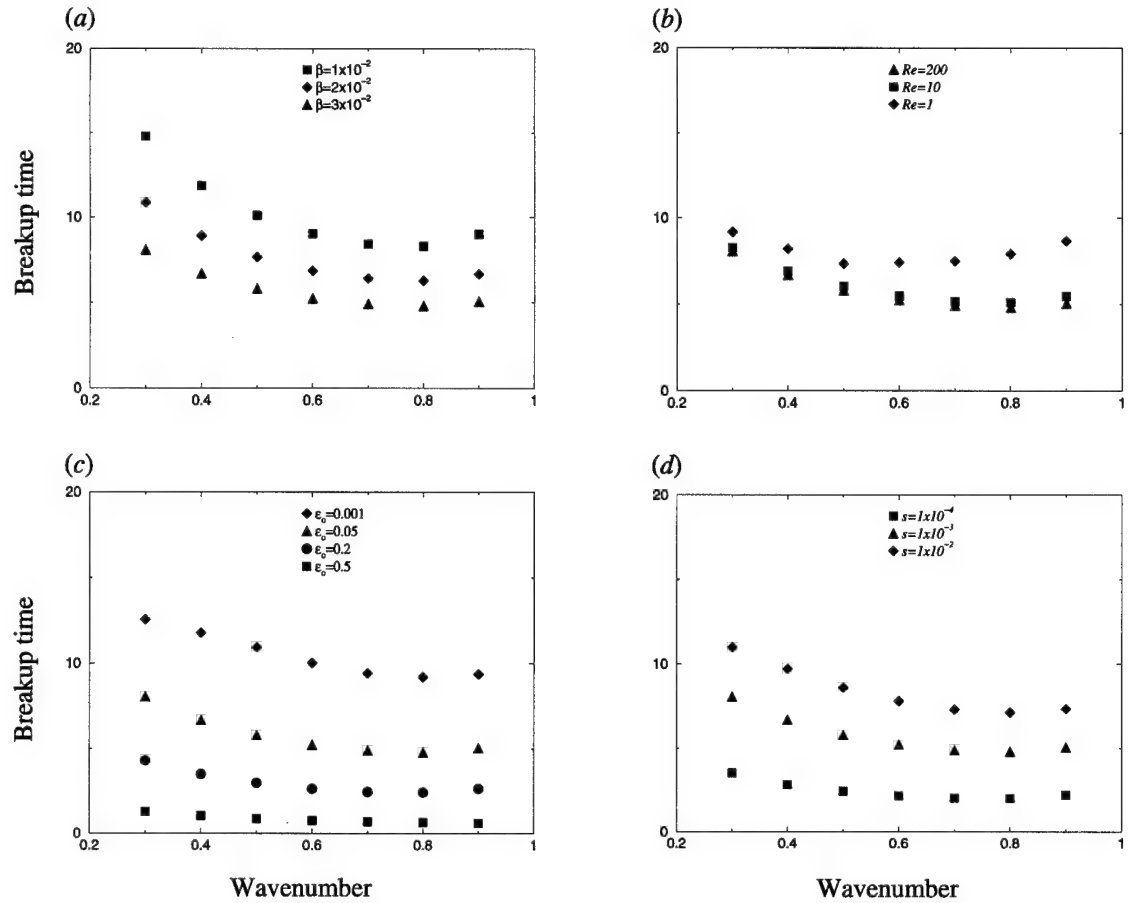

Figure 7: Breakup time of jet: (*a*) Re=200,ε_o=0.05,s=10^{-3}; (*b*) ε_o=0.05,β=3x10^{-2},s=10^{-3}; (*c*) Re=200,β=3x10^{-2},s=10^{-3}; (*d*) Re=200,ε_o=0.05,β=3x10^{-2}.

previous observation for non-evaporating jets in the Reyleigh regime (Mashayek and Ashgriz 1995). Another important point to note is that the minimum breakup time shifts to lower wavenumbers as Re is significantly reduced. This is in accordance to linear theory which states that the maximum growth rate shifts toward the lower wavenumbers for more viscous liquid jets. Even though our cases involve evaporation, Fig. 7c still re-emphasizes Chaudhary's results by showing that as ε_o increases from zero the minimum breakup time occurs at higher wavenumbers. For example, for ε_o=0.5 the minimum breakup time occurs at k=0.9 but for

ε_o=0.001 this happens at k=0.8. Clearly, from Fig. 7c we notice as initial disturbance amplitude increases breakup time decreases. From inspection of Fig. 7d we can dissimulate that an increase in density ratio increases breakup time due to the diminishing of the recoil force.

Breakup volume, the instantaneous combined volume of both the main drop and the satellite drop at breakup, is primarily dependent on jet breakup time. If it takes longer for jet breakup to occur then the jet is allowed more time to evaporate. Beginning with an initial normalized jet volume of one, Fig. 8 shows the final volume of the jet while varying different parameters. Analysis of the results from each graph gives similar conclusions to that described for the breakup time.

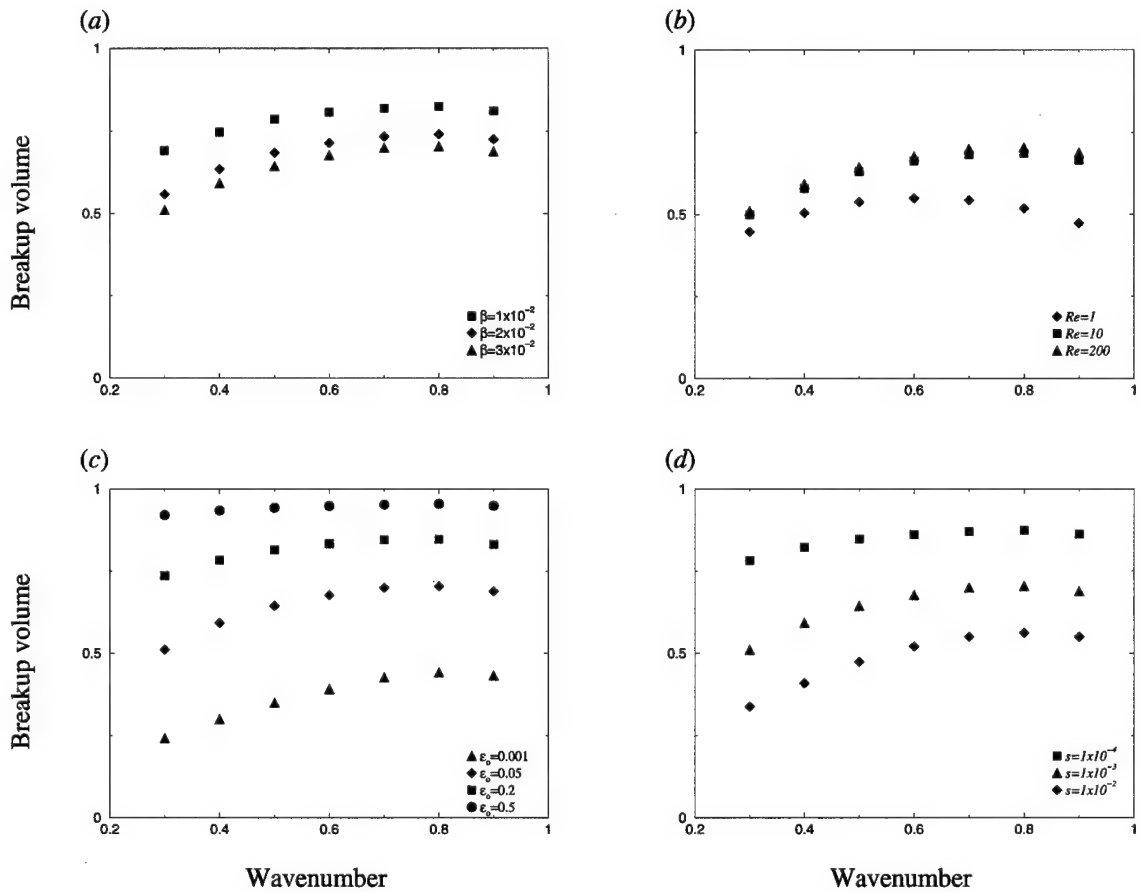

Figure 8: Breakup volume of jet: (*a*) Re=200,ε_o=0.05,s=10^{-3}; (*b*) ε_o=0.05,β=3x10^{-2},s=10^{-3}; (*c*) Re=200,β=3x10^{-2},s=10^{-3}; (*d*) Re=200,ε_o=0.05,β=3x10^{-2}.

3.4 Drop size at breakup

The control of satellite drops has been one of the primary driving forces behind nonlinear jet instability studies. For non-evaporating jets the total volume of a single wavelength of fluid is constant throughout the breakup process and equal to the combination of the main drop volume and satellite drop volume at breakup. However for evaporating jets the volume changes in time and the total volume of the jet at any instant is equal to the initial jet volume minus the total amount of evaporation up to that point. At breakup, the volume of an evaporating jet is equal to the combined volume of both the main and satellite drops, where this total could be significantly less than the initial volume depending on the evaporation rate and the breakup time.

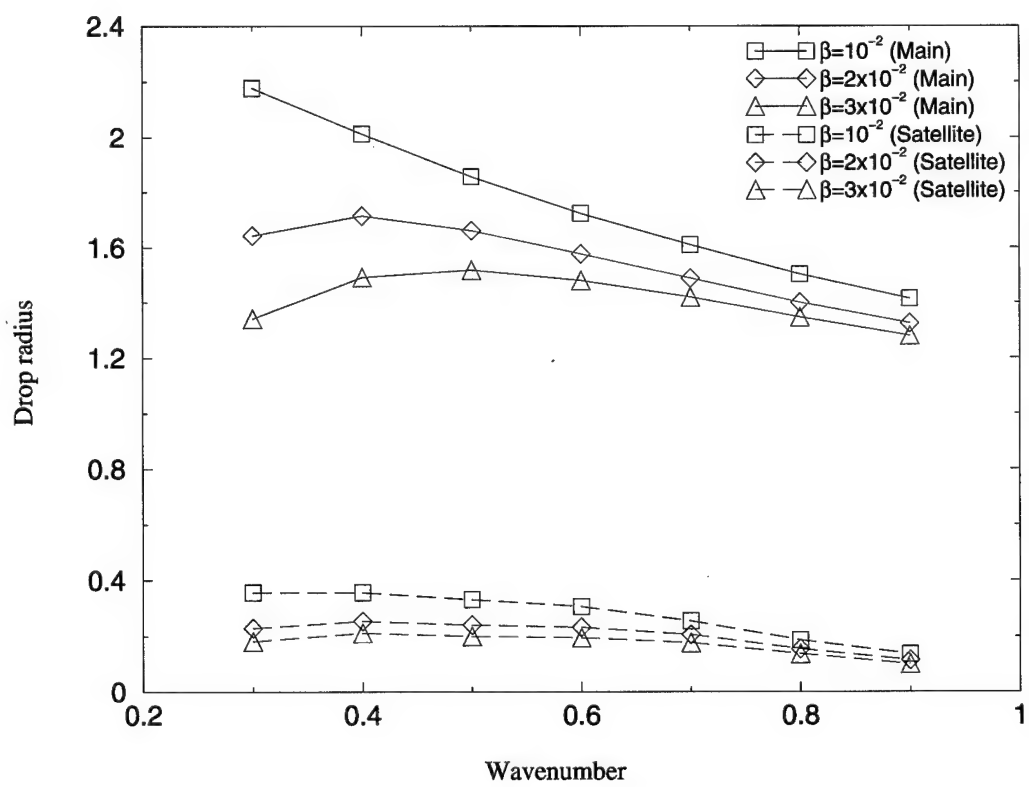

Figure 9: Variation of drop size at breakup, Re=200,ε_o=0.05,s=10^{-3}.

Figure 9 plots the main and satellite drop radii versus wavenumber for $\beta=10^{-2},2x10^{-2},3x10^{-2}$. From this figure we see that, for small evaporation rate, as wavelength increases the drop size generally increases, which is similar to non-evaporating jets. However, large evaporation rates and small wavenumbers (i.e. k=0.3 for $\beta=2x10^{-2}$ and k=0.3,0.4 for $\beta=3x10^{-2}$) we notice a decrease in both main and satellite drop size due to the increased breakup time, which allows more vapor to leave the surface and reduce the overall jet volume. Two general conclusions from Fig. 9 are: (i) as evaporation rate increases drop size decreases for all disturbance wavenumbers, and (ii) comparing the percent reduction in drop size evaporation affects the satellite drop more than the main drop (e.g. by increasing β by a factor of 3 at k=0.3 the main drop radius reduces 38% and the satellite drop radius reduces 50%, or at k=0.9 this reduces the main drop by 10% and the satellite drop by 29%).

3.5 Evaporation flux on free surface

In our evaporation model we approximate the unit area evaporation rate of our perturbed jet surface with that of a sphere with the same local radius of curvature. Curvature of the jet surface is determined by the height function using (15). To be in agreement with (9) the curvature of the surface was monitored throughout simulations to prohibit negative values in evaporation cases. Figure 10 shows the curvature of the jet versus the axial coordinate z for the simulations presented in Fig. 2. In every case the curvature increases in the neck region as we approach the breakup time. This translates to an increase in the evaporation mass flux as shown in (26). That is, the evaporation flux at the neck is higher than that at the swell, leading to further pinching of the neck. Also the recoil force is stronger in the neck region than that at the

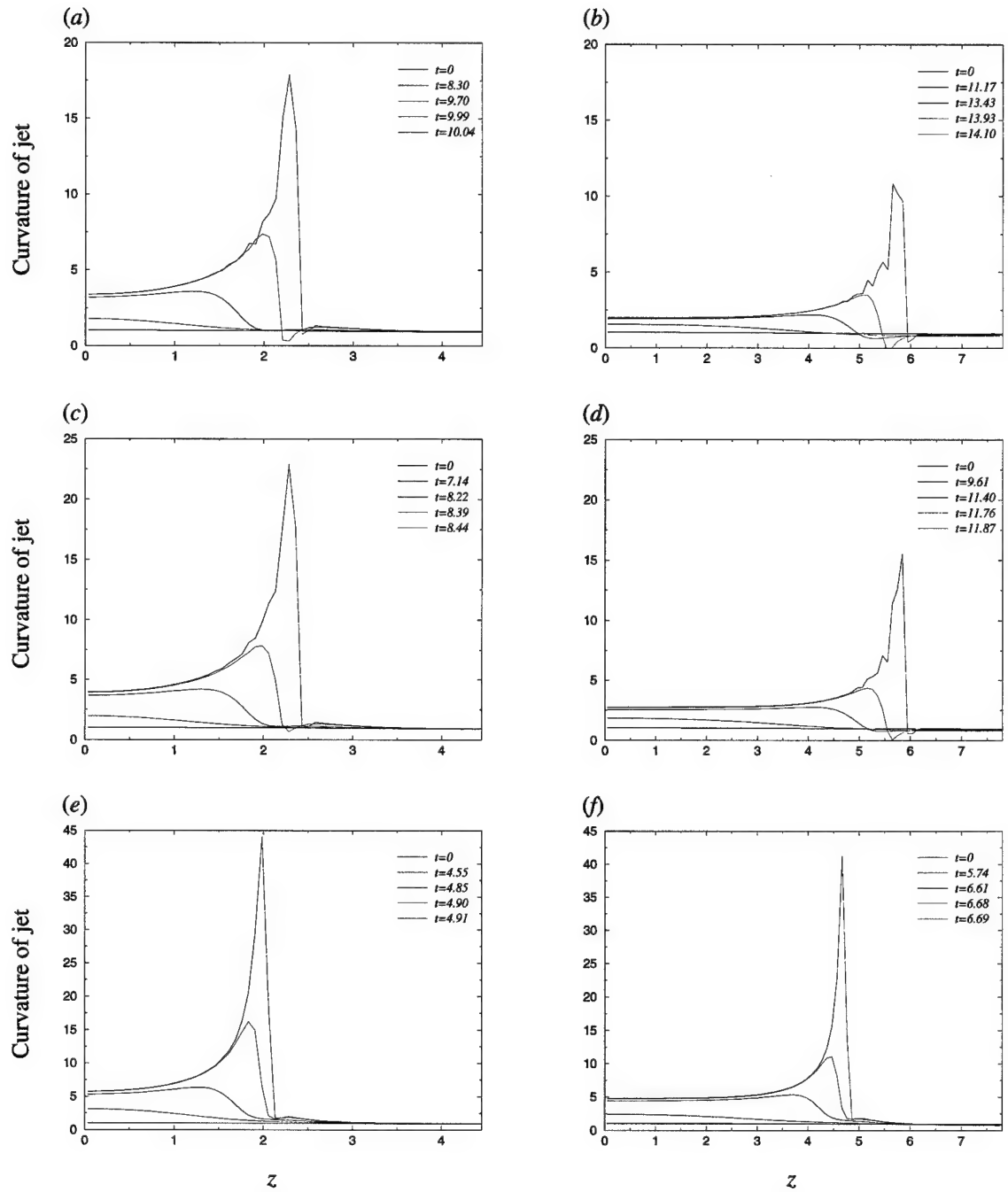

Figure 10: Variation of the curvature of the jet, Re=200, ε_o=0.5, s=10^{-3}: (*a*) k=0.7, β=0; (*b*) k=0.4, β=0; (*c*) k=0.7, β=1x10^{-2}; (*d*) k=0.4, β=1x10^{-2}; (*e*) k=0.7, β=3x10^{-2}; (*f*) k=0.4, β=3x10^{-2}.

crest, causing the liquid to be squeezed into the crests and thus accelerating the growth of the disturbance at the neck. The point of highest curvature in each set of data represents the

instantaneous minimum radius of curvature. At the breakup time we see a drastic increase in the curvature which is associated with the breakup point. By investigating Fig. 10a,c,e we can easily see that the breakup point is closer to the neck for increasing evaporation rates.

3.6 Pressure and velocity distributions

To provide further insight into the dynamics of the jet the velocity and pressure distributions within the liquid jet have been investigated. Figure 11 shows the pressure distribution and velocity vectors at three different non-dimensional times for a non-evaporating jet. At all the times shown we can easily see the flow of the fluid from the neck to the swell. With increasing surface deformation a significant increase of velocity in the neck region takes place. Initially the pressure distribution is uniform within the jet but as the velocity field develops we can clearly identify areas of low and high pressure. At the final time shown, which is near the breakup time, we can distinguish a high-pressure region at the top of the swell due to the conversion of velocity to pressure. The middle ligament exhibits a lower pressure where the velocities are higher. For comparison Fig. 12 gives the results for an evaporating jet with similar parameters as Fig. 11. From the legend we see that the evaporating case produces a higher overall pressure, which is due to the contribution of both capillary and recoil forces. We can clearly identify the recoil force in both the middle ligament and the main drop of our jet where we see a higher pressure along the surface. It should be mentioned that in Figs. 11 and 12 the velocity vectors have been scaled in each of the 3 non-dimensional times for clarity.

By increasing the disturbance wavelength and decreasing the initial disturbance amplitude our code has been able to predict multiple satellite drops, which has been investigated

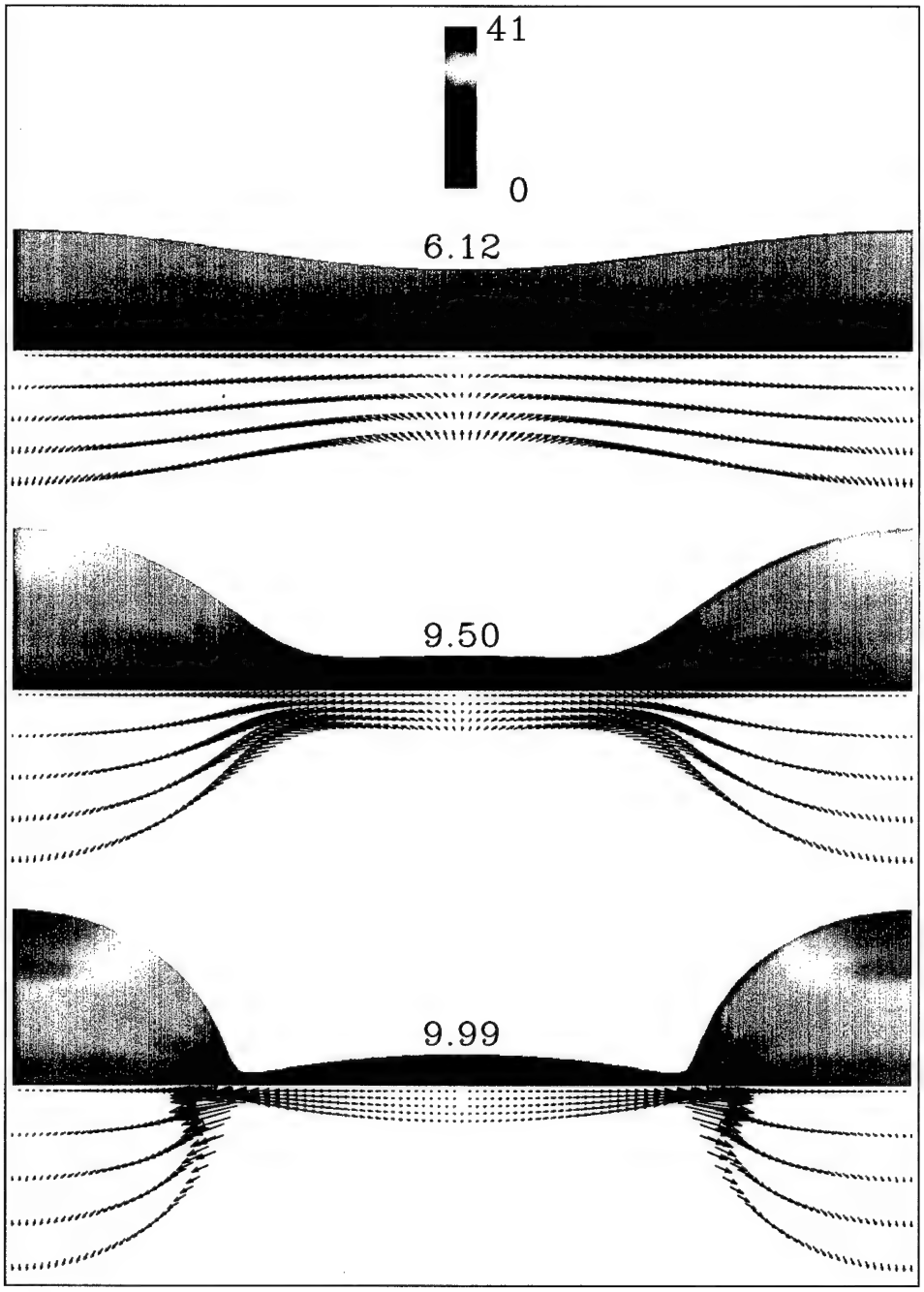

Figure 11: Pressure distribution and velocity vectors for a non-evaporating jet, Re=200, k=0.7, ε_o=0.05, β=0, s=10^{-3}.

experimentally by Vassallo and Ashgriz (1991). Figures 13 and 14 give insight into the differences seen between non-evaporating and evaporating jets under these conditions. From the

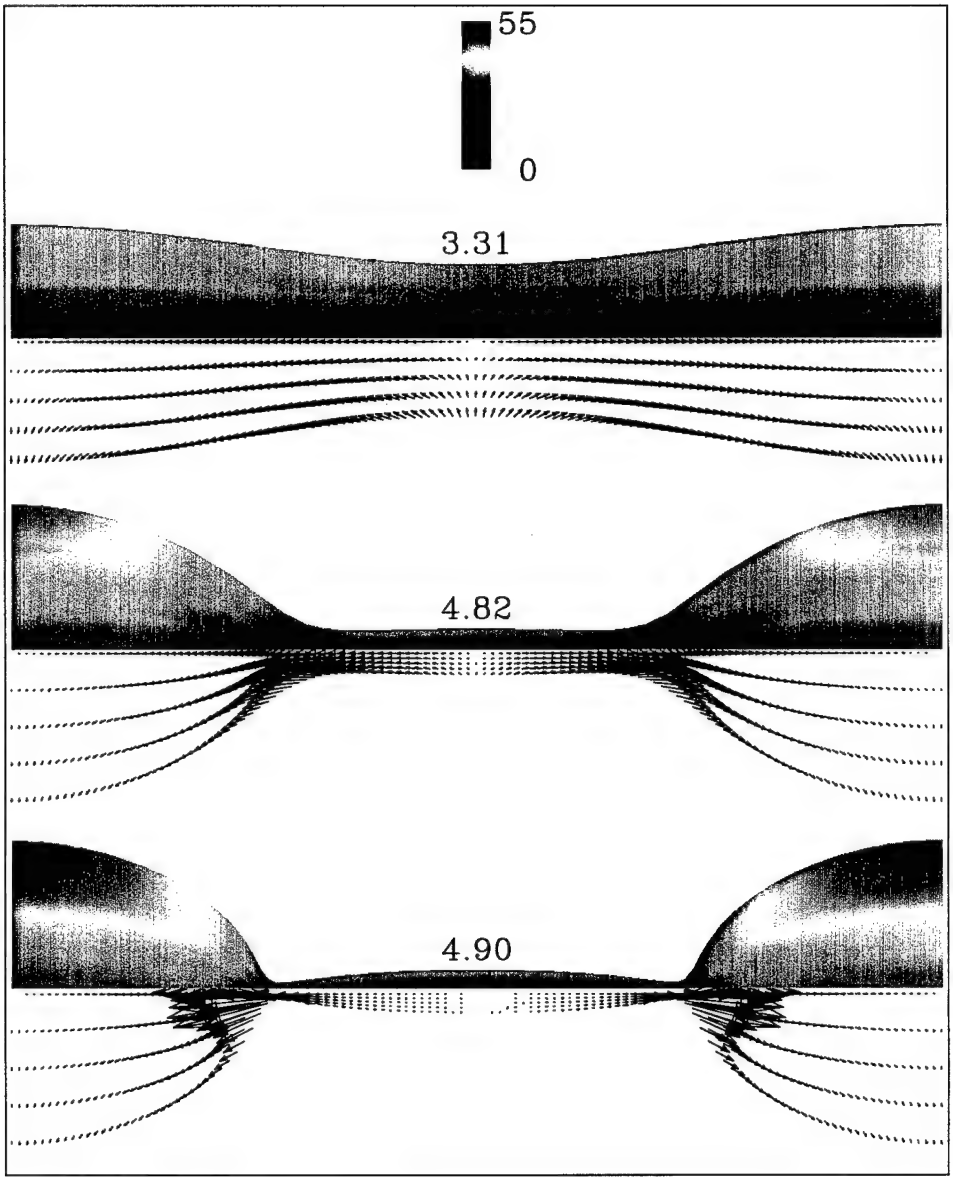

Figure 12: Pressure distribution and velocity vectors for an evaporating jet, Re=200, k=0.7, ε_o=0.05, β=3x10^{-2}, s=10^{-3}.

non-evaporating case, Fig. 13, we notice that nonlinear effects have drastically influenced the surface shape near breakup. Here we can identify a main drop and, possibly, multiple satellite drops which after breakup would either combine and oscillate or separate. Investigating Fig. 14

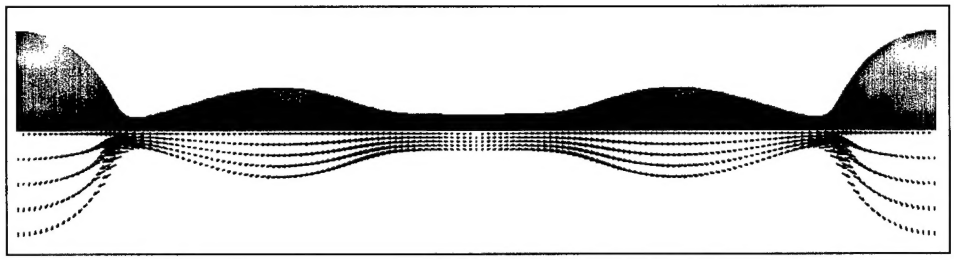

Figure 13: Formation of multiple satellite drops for a non-evaporating jet, Re=200, k=0.3, ε_o=0.001, β=0, s=10^{-3}.

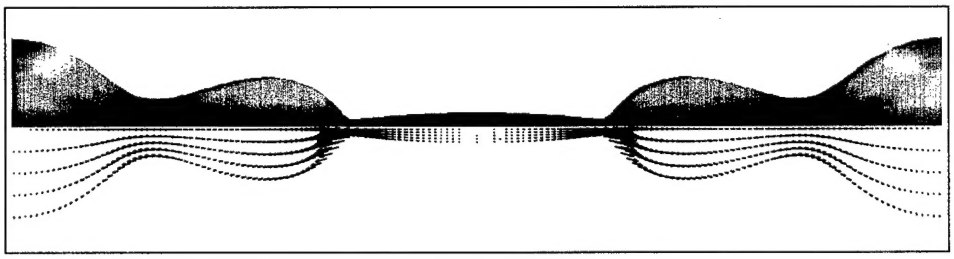

Figure 14: Formation of multiple satellite drops for an evaporating jet, Re=200, k=0.3, ε_o=0.001, β=10^{-3}, s=10^{-3}.

for evaporating case, we see a different surface shape due to the relocation of the breakup point close to the initial neck. This jet creates one small liquid ligament and two larger bulged volumes of liquid, which would continue to interact after breakup.

4. Conclusion

Numerical simulation is used to investigate the instability of evaporating capillary jets. The evaporation model is based on the d^2-law, widely used for spherical drops. To implement this model for perturbed jets, the conventional d^2-law is modified by substituting the local radius

of the surface for the radius of a sphere. The need for a solution for the ambient gas is eliminated considering small density ratios. Numerical simulations are carried out using a Galerkin finite element method with penalty function. The motion of the free surface is tracked using the Height-Flux Method developed by Mashayek and Ashgriz (1993). With this technique, the evaporation at the surface is easily handled by modifying the amount of fluid within each subvolume. Preliminary simulations were performed to establish the required mesh size and time increment for various cases.

In non-dimensional form, the formulation involves five parameters: the amplitude of the initial surface disturbance, the wavenumber of the initial surface disturbance, the Reynolds number, the non-dimensional evaporation rate, and the density ratio. A wide range of variation for each of these parameters is considered in numerical simulation. The results were discussed for various cases leading to the foremost conclusion that evaporation clearly has an effect on jet instability, mainly increasing the growth rate of the disturbances by increasing the evaporation flux at the neck. Thus, evaporation causes the jet to break up sooner and reduces the size of both main and satellite drops. An increase in internal pressure is also noticed with evaporating cases due to the contribution of both capillary and recoil forces. Due to the limited number of evaporating jet instability studies the majority of our conclusions could not be compared to experimental or analytical results.

References

Bogy, D. B., *Drop Formation in a Circular Liquid Jet*, Ann. Rev. Fluid Mech., 11:207-228 (1979).

Chandrasekhar, S., *Hydrodynamic and Hydromagnetic Stability*, Claredon, Oxford, (1961).

Chaudhary, K. C. and Redekopp, L. G., *The Nonlinear Capillary Instability of a Liquid Jet. Part 1*, J. Fluid Mech., 96(2): 257-274 (1980).

Eggers, J., *Nonlinear Dynamics and Breakup of Free-surface Flows*, Rev. Modern Phys, 69(3):865-929 (1997).

Eggers, J. and Dupont, T. F., *Drop Formation in a One-dimensional Approximation of the Navier-Stokes Equation*, J. Fluid Mech., 262:205-221 (1994).

Goedde, E. F. and Yuen, M. C., *Experiments on liquid jet instability*, J. Fluid Mech., 40(3):495-511 (1970).

Hughes, T.J.R., Liu, W.K., and Brooks, A, *Finite Element Analysis of Incompressible Viscous Flows by the Penalty Function Formulation*, J. Comput. Phys., 30:1-60 (1979).

Kowalewski, T. A., *On the Separation of Droplets of a Liquid Jet*, Fluids Dyn. Res., 17(3):121 (1996).

Lian, Z. W. and Reitz, R. D., *The Effect of Vaporization and Gas Compressibility on Liquid Jet Atomization*, Atomization and Sprays, 3:249-264 (1993).

Mansour, N. N. and Lundgren, T. S., *Satellite Formation in Capillary Jet Breakup*, Phys. Fluids A, 2:1141-1144 (1990).

Mashayek, F. and Ashgriz, N., *A Height-Flux Method for Simulating Free Surface Flows and Interfaces,* Int. J. Num. Methods Fluids, 17:1035-1054 (1993).

Mashayek, F. and Ashgriz, N., *Temporal Analysis of Capillary Jet Breakup*, J. Fluid Mech., 291:163-190 (1995).

Rayleigh, W. S., *On the Instability of Jets*, Proc. London Math. Soc., 10:4-13 (1879).

Stone, H. A. and Leal, L. G., *The Influence of Initial Deformation on Drop Breakup in Subcritical Time-dependent Flows at Low Reynolds Number*, J. Fluid Mech., 206:223-263 (1989).

Tsai, W. T. and Yue, D. K. P., *Computation of Nonlinear Free-surface Flows*, Annu. Rev. Fluid Mech., 28:249-278 (1996).

Turns, S. R., *An Introduction to Combustion: Concepts and Applications*, McGraw Hill Inc., (1996).

Vassallo, D. P. and Ashgriz, N., *Satellite Formation and Merging in Liquid Jet Breakup*, Proc. R. Soc. Lond. A, 433:269-286 (1991).

Weber, C. Z., *Zum Zerfall eines Flussigkeitsstrahles*, Angew. Math. Mech., 11:136-154 (1931).

Williams, F. A., *Combustion Theory*, The Benjamin/Cummings Publishing Co., Menlo Park, CA, 2nd ed., (1985).

Yuen, M.C., *Non-linear Capillary Instability of a Liquid Jet*. J. Fluid Mech., 33:151-163 (1968).